arXiv:1610.05535v1 [physics.chem-ph] 18 Oct 2016

FMO3-LCMO study of electron transfer coupling matrix element and pathway: Application to hole transfer between two triptophanes through cis- and trans-polyproline-linker systems

Hirotaka Kitoh-Nishioka* and Koji Ando†
Department of Chemistry, Graduate School of Science, Kyoto University, Sakyo-ku, Kyoto 606-8502, Japan

The linear-combination of fragment molecular orbitals with three-body correction (FMO3-LCMO) is examined for electron transfer (ET) coupling matrix elements and ET pathway analysis, with application to hole transfer between two triptophanes bridged by cis- and trans-polyproline linker conformations. A projection to the minimal-valence-plus-core FMO space was found to give sufficient accuracy with significant reduction of computational cost while avoiding the problem of linear dependence of FMOs stemming from involvement of bond detached atoms.

I. INTRODUCTION

Long-distance electron transfer (ET) plays an essential role in biological energy conversion [1–5]. Representative are those in photosynthetic reaction centers in which photon energy is converted to electrochemical energy via series of ETs through redox centers embedded in transmembrane protein. A simple but fundamental question open to microscopic investigation is how the protein environment is involved in the ET: the protein structure could be involved passively by simply holding the redox centers at appropriate spatial configuration, or actively by providing intermediate virtual states for superexchange ET mechanism [6].

To address this and related questions, quantum mechanical investigation based on realistic molecular structure is essential. However, first-principles treatment of electrons in large biomolecular systems is still a formidable task. In this regard, fragment-based approaches, such as the fragment molecular orbital (FMO) [7–9], Divide-and-Conquer [10, 11], and many others [12–15] appear promising.

In a series of papers, we have reported calculations of ET coupling matrix element and ET pathways [16–18] from the linear-combination of FMOs (FMO-LCMO) [19] with the two-body correction (FMO2). The method was found to give accurate ET couplings over four orders of magnitude along the ET distance when the bond detached atoms (BDA) were not involved or when the minimal atomic basis set was used [16]. Nevertheless, the problem of degraded MO energies caused by BDAs with atomic basis sets larger than minimal set, that had been already pointed out in Ref. [19], carried over to the ET analysis. Recently, however, Kobori et al. have found notable remedy of MO energies with the three-body correction (FMO3) [20]. Following this, we study in this work how the FMO3 correction affects the ET coupling energy and ET pathway analysis.

We also examine selection of the FMO space. In Ref. [20], in order to remove linear dependence of basis functions associated with BDAs, a canonical transformation of Hamiltonian matrix,

$$\tilde{H} = U^{\dagger} H U, \tag{1}$$

where the matrix U diagonalizes overlap matrix, was employed. However, this transformation often mixes the FMOs in unwanted ways for the ET pathway analysis, particularly for studying inter-fragment tunneling current. We found that the problem can be evaded by a projection to restricted FMO space instead of the canonical transformation of Eq. (1). For instance, with FMO-LC(VC)MO scheme, which restricts to the minimal-valence (V) plus core (C) MO space, the smallest eigenvalue of overlap matrix for systems studied in this work was 0.225, which is large enough to regard the FMO space linearly independent [21].

For numerical demonstration, we examine hole transfer between two triptophane (Trp) residues bridged by helical polyproline oligopeptide, which serves a good model of long-distance ETs observed in metal-derivatized oligoprolines [22–24]. Previous theoretical works [25, 26] have employed the same model systems to study the effects of solvent and bridge-conformation dynamics on the electronic coupling.

Section II outlines the theoretical framework. Section III describes the computational details. Applications to hole transfer between two Trp molecules bridged by polyproline linker systems are discussed in Sec. IV. Section V concludes.

II. THEORY

A. FMO-LCMO and projection to restricted FMO space

Here we outline the FMO-LCMO method [19, 20] to explain the present projection scheme to the restricted FMO space.

The FMO-LCMO Hamiltonian up to the three-body FMO3 correction is described as

$$H_{\text{total}}^{\text{FMO3}} = H_{\text{total}}^{\text{FMO1}} + \Delta H_{\text{total}}^{\text{FMO2}} + \Delta H_{\text{total}}^{\text{FMO3}}, \tag{2}$$

in which $H_{\text{total}}^{\text{FMO1}}$ consists of monomer Fock matrices, and $\Delta H_{\text{total}}^{\text{FMO2}}$ and $\Delta H_{\text{total}}^{\text{FMO3}}$ are the two- and three-body corrections. The intra-fragment block of $\Delta H_{\text{total}}^{\text{FMO2}}$, between FMOs ϕ_p^I and ϕ_q^I in the same fragment I, is given by

$$(\Delta H_{\text{total}}^{\text{FMO2}})_{I_p,I_q} = \sum_{J\neq I} \{(H_{I\leftarrow IJ})_{I_p,I_q} - (H_{I\leftarrow I})_{I_p,I_q}\}, \tag{3}$$

*Present address: Center for Computational Sciences, University of Tsukuba, E-mail: hkito@ccs.tsukuba.ac.jp
†E-mail: ando@kuchem.kyoto-u.ac.jp

whereas the inter-fragment block is

$$(\Delta H^{\rm FMO2}_{\rm total})_{I_p,J_q} = (H_{IJ\leftarrow IJ})_{I_p,J_q}. \quad (4)$$

The terms in the right-hand-side of Eqs. (3) and (4) will be defined in Eqs. (7)–(9).

The FMO3 correction to the intra- and inter-fragment blocks are

$$(\Delta H^{\rm FMO3}_{\rm total})_{I_p,I_q} = \sum_{J<K}\sum_{J,K\neq I}\{(H_{I\leftarrow IJK})_{I_p,I_q} - (H_{I\leftarrow IJ})_{I_p,I_q} - (H_{I\leftarrow IK})_{I_p,I_q} + (H_{I\leftarrow I})_{I_p,I_q}\} \quad (5)$$

and

$$(\Delta H^{\rm FMO3}_{\rm total})_{I_p,J_q} = \sum_{K\neq I,J}\{(H_{IJ\leftarrow IJK})_{I_p,J_q} - (H_{IJ\leftarrow IJ})_{I_p,J_q}\}. \quad (6)$$

As noted in Introduction, the canonical transformation of Eq. (1) is not desired for the ET pathway analysis. We thus simply limit the number of FMOs and project the Hamiltonian matrix to this set. We denote this "restricted FMO (rFMO)" space. Therefore, the terms in the right-hand-side of Eqs. (3)–(6) in the selected rFMO space $\{\phi^I_p\}$ are defined as follows. With the fragment monomer, dimer, and trimer represented by $X = I, IJ$, and IJK, the intra-fragment blocks are defined by

$$(H_{I\leftarrow I})_{I_p,I_q} = \varepsilon_{I_p}\delta_{I_p,I_q} \quad (7)$$

and

$$(H_{I\leftarrow X})_{I_p,I_q} = \sum_{X_r}\langle\phi^I_p|\phi^X_r\rangle\varepsilon^X_r\langle\phi^X_r|\phi^I_q\rangle, \quad (8)$$

whereas the inter-fragment blocks are

$$(H_{IJ\leftarrow X})_{I_p,J_q} = \sum_{X_r}\langle\phi^I_p|\phi^X_r\rangle\varepsilon^X_r\langle\phi^X_r|\phi^J_q\rangle. \quad (9)$$

In the summation over X_r in the right-hand-side, all the dimer and trimer FMOs are taken, except the spurious ones stemming from the BDAs.

B. ET coupling and pathway analysis

To calculate the ET coupling matrix element $T_{\rm DA}$, we employ two methods; generalized Mulliken-Hush (GMH) [27] and bridge Green function (BGF) [28–30].

The GMH method scales the donor-acceptor MO energy splitting $\Delta\varepsilon_{\rm DA}$ by a formula

$$T_{\rm DA} = \frac{|\mu_{\rm DA}|\ \Delta\varepsilon_{\rm DA}}{\sqrt{(\mu_{\rm D}-\mu_{\rm A})^2 + 4|\mu_{\rm DA}|^2}}, \quad (10)$$

in which $\mu_{\rm D}$, $\mu_{\rm A}$ and $\mu_{\rm DA}$ are the diagonal and off-diagonal dipole matrix elements. It assumes that the Hamiltonian and dipole matrix elements scale similarly for states involved in ETs. Despite its simplicity, the GMH formula (10) has been successfully applied to a number of ET reactions.

The BGF method has been also demonstrated to give accurate and robust results with

$$T_{\rm DA} = H^{\rm direct}_{\phi_{\rm D},\phi_{\rm A}} + \sum_{I,J}^{N}{\sum_{I_p,J_q}}'(E_{\rm tun}S_{\phi_{\rm D},I_p} - H_{\phi_{\rm D},I_p}) \times G^{\rm B}(E_{\rm tun})_{I_p,J_q}(E_{\rm tun}S_{J_q,\phi_{\rm A}} - H_{J_q,\phi_{\rm A}}), \quad (11)$$

in which the sums over I_p and J_q exclude donor and acceptor MOs, $\phi_{\rm D}$ and $\phi_{\rm A}$. The first term in the right-hand-side is the direct coupling between $\phi_{\rm D}$ and $\phi_{\rm A}$. S is the overlap matrix. $G^{\rm B}(E)$ is the bridge Green function defined as

$$G^{\rm B}(E) = (ES_{QQ} - H_{QQ})^{-1}, \quad (12)$$

in which Q is the projection operator to the MO space external to the donor-acceptor MOs. The electron tunneling energy $E_{\rm tun}$ is naturally defined as the average of donor-acceptor orbital energies, $E_{\rm tun} = (\varepsilon_{\rm D} + \varepsilon_{\rm A})/2$.

In the tunneling current analysis [30, 31], the ET coupling $T_{\rm DA}$ is expressed as a sum of tunneling current $\mathcal{J}_{I_p,J_q}$ between basis FMOs $\{\phi^I_p\}$ [16, 17],

$$T_{\rm DA} = \hbar\sum_{I\in\Omega_{\rm D}}\sum_{J\notin\Omega_{\rm D}}\mathcal{J}_{I,J}, \quad (13)$$

$$\mathcal{J}_{I,J} = \sum_{I_p}\sum_{J_q}\mathcal{J}_{I_p,J_q}, \quad (14)$$

in which the summation over I_p and J_q are over the FMOs within fragments I and J, and $\Omega_{\rm D}$ denotes the spatial region assigned to the donor molecule. The inter-orbital current $\mathcal{J}_{I_p,J_q}$ is computed from the electronic Hamiltonian and overlap matrices and the coefficients of FMO-LCMO, $\{C^{\rm i}_{I_p}\}$ and $\{C^{\rm f}_{I_p}\}$, that represent the mixing of bridge FMOs to the donor and acceptor FMOs, $\phi_{\rm D}$ and $\phi_{\rm A}$, in the initial (i) and final (f) states, $\psi^{\rm i}$ and $\psi^{\rm f}$,

$$|\psi^{\rm i}\rangle = C^{\rm i}_{\rm D}|\phi_{\rm D}\rangle + \sum_{I}^{N}\sum_{I_p}C^{\rm i}_{I_p}|\phi^I_p\rangle, \quad (15)$$

$$|\psi^{\rm f}\rangle = C^{\rm f}_{\rm A}|\phi_{\rm A}\rangle + \sum_{I}^{N}\sum_{I_p}C^{\rm f}_{I_p}|\phi^I_p\rangle, \quad (16)$$

$$\mathcal{J}_{I_p,J_q} = \frac{1}{\hbar}\left(H_{I_p,J_q} - E_{\rm tun}S_{I_p,J_q}\right)\left(C^{\rm i}_{I_p}C^{\rm f}_{J_q} - C^{\rm f}_{I_p}C^{\rm i}_{J_q}\right). \quad (17)$$

These are thus computed straightforwardly from the FMO-LCMO method. The normalized inter-fragment tunneling current is defined by

$$\mathcal{K}_{I,J} = \hbar\mathcal{J}_{I,J}/T_{\rm DA}, \quad (18)$$

which satisfies

$$\sum_{I\in\Omega_{\rm D},J\notin\Omega_{\rm D}}\mathcal{K}_{I,J} = 1. \quad (19)$$

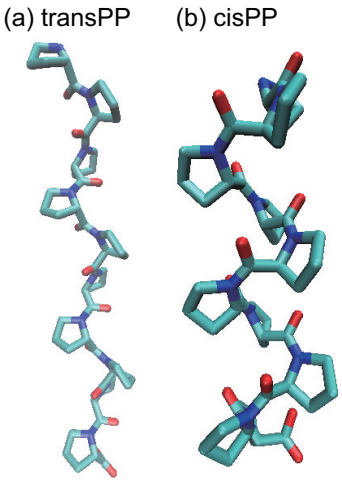

FIG. 1: Schematic drawings of the helix structures of polyproline linker with (a) trans- and (b) cis-configurations.

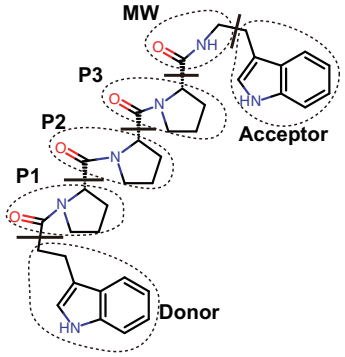

FIG. 2: Fragments in polyproline linker. P1-3 are three proline residues and MW denotes the main chain of Trp (W).

Table I. Number of MOs in the rFMO spaces.

	D	P1	P2	P3	MW	A	Total
Occupied	38	26	26	26	15	35	166
LC(VC)MO	64	42	42	42	23	59	272[a]
Full	184	129	129	129	76	177	824 (774[b])

[a]Corresponds to the minimal set.
[b]Without BDAs.

III. COMPUTATION

A. Polyproline linker conformation

For the purpose of benchmarking the FMO3-LCMO calculations, we consider proline-trimer bridged systems, Trp-(Pro)$_3$-Trp, with two types of helix structure of polyproline (PP) linker, one with cis-configurations (cisPP) and the other with trans-configurations (transPP) of peptide bonds. The former and latter proline trimers have the backbone dihedral angles (φ, ψ) of approximately $(-75°, 150°)$ and $(-75°, 160°)$, respectively. The cisPP and transPP structures are schematically drawn in Fig. 1. Apparently the transPP is more stretched.

Starting from typical conformations of cisPP and transPP, local strains were removed by geometry optimization at the B3LYP/6-31G(d)-D3 level, with the D3 version of Grimme's dispersion correction with the original D3 damping function [32]. We used Gaussian09 program [33] for the geometry optimization. The resultant molecular structures are displayed in Fig. S1 and Table S1 of the Supplementary Material.

B. FMO calculation

In the FMO calculation, the Trp-(Pro)$_3$-Trp chain was divided into six fragments as designated in Fig. 2, in which P1-P3 are the three prolines and MW denotes the Main-chain of Trp (W). The α-carbon atoms were treated as BDAs. The HOMOs of Trp fragments were taken as the donor and acceptor MOs of hole transfer. The electronic coupling and tunneling current from the FMO2-LCMO and FMO3-LCMO methods were compared to a reference calculation with the RHF Hamiltonian of the entire system of six fragments projected to the FMO space. We denote this last scheme FMO6-LCMO with the Hamiltonian matrix

$$(H^{\mathrm{FMO6}}_{\mathrm{total}})_{I_p,J_q} = \sum_a \langle \phi^I_p | \psi_a \rangle \varepsilon_a \langle \psi_a | \phi^J_q \rangle, \qquad (20)$$

where ϕ^I_p, ϕ^I_q are MOs in the rFMO space and ψ_a and ε_a are the MOs and MO energies of the entire system.

We consider a "minimal-valence plus core" rFMO space that includes the same number of MOs as the minimal basis set such as STO-3G. We denote this LC(VC)MO space. Other choices of rFMO space, LUMO, LUMO+2, LUMO+6, LUMO+10, to check the dependence on the size of rFMO space, are obtained by augmenting the lower unoccupied MOs of each fragment to the occupied space.

The 6-31G(d) basis set was used. The total number of basis AOs for the entire system is 774. The FMO2 and FMO3 calculations include additional 50 AOs from the BDAs. The number of FMOs in the occupied, LC(VC)MO, and full spaces for each fragment are summarized in Table I. For basis sets larger than the double-zeta basis, the LC(VC)MO scheme gives significant reduction. Moreover, it removed the problem of linear-dependence observed previously [20], as the smallest eigenvalue of the overlap matrix in the LC(VC)MO space was 0.225.

We used the program GAMESS [34] for the conventional FMO calculation [35]. To estimate all inter-fragment tunneling currents including the long-distance ones, we did not employ the electrostatic dimer (ES-DIM) approximation [36] that avoids self-consistent field calculations of the far separated dimers in FMO calculations.

Table II. MO energy gap and errors (in eV) of transPP helix from FMO-LC(VC)MO calculations.

	Gap[a]	MAE[b]		RMS[c]	
		Occ	Uoc	Occ	Uoc
FMO2	10.66	0.107 (#15)	22.4 (#272)	0.0345	3.92
FMO3	10.67	0.102 (#27)	14.6 (#272)	0.0266	3.13
FMO6	10.63	0.0934 (#65)	14.6 (#272)	0.0223	3.13

[a]HOMO-LUMO gap. The reference RHF value is 10.63 eV.
[b]Maximum absolute error of MO energies. Occ / Uoc denote occupied / unoccupied MOs. In parentheses are the MO numbers that exhibit the MAE.
[c]Root-mean-square error of MO energies.

Table III. Same as Table II but for cisPP helix.

	Gap[a]	MAE		RMS	
		Occ	Uoc	Occ	Uoc
FMO2	9.885	0.271 (#19)	22.18 (#272)	0.0504	3.74
FMO3	9.890	0.0988 (#40)	14.89 (#272)	0.0227	3.12
FMO6	9.909	0.0863 (#65)	14.95 (#272)	0.0213	3.14

[a]The reference RHF value is 9.904 eV.

IV. RESULTS

A. Errors in MO energy

The diagonalization of the FMO-LCMO Hamiltonian matrix can provide approximate canonical MOs and corresponding energies for the entire system [19, 20]. First we assess accuracy of the FMO-LC(VC)MO method with regard to the MO energies. The computed errors from the RHF calculation of the entire system are summarized in Tables II and III for transPP and cisPP, respectively. For the occupied MOs, the maximum absolute error (MAE) was observed at different MO numbers for FMO2, FMO3, and FMO6 calculations (for instance, Nos. 15, 27, and 65 for transPP) but these commonly involve the BDA. The MAE of unoccupied MOs was always observed at the highest MO (No. 272). The root-mean-squares error is notably reduced from FMO2 to FMO3, but not so much from FMO3 to FMO6, indicating nearly converged accuracy at the FMO3 level.

B. ET coupling energy

Next we examine the ET coupling matrix element $T_{\rm DA}$. Figure 3 displays the computed $T_{\rm DA}$ with varying rFMO spaces, from the "occupied-only" to the minimal-valence plus core (VC). The numerical values are listed in Tables IV and V. The absolute value of $T_{\rm DA}$ is about 20 times larger for cisPP than transPP because of the shorter donor-acceptor distance in the former. As seen in Fig. 3(a), the $T_{\rm DA}$ in transPP converge to the value of full space with an oscillation. The behavior for cisPP in Fig. 3(b) is less simple; the results of FMO2 exhibit notable oscillation which is less prominent in FMO3 and FMO6. For both cisPP and transPP, FMO3 notably improves the $T_{\rm DA}$ value over FMO2 and has been almost converged to

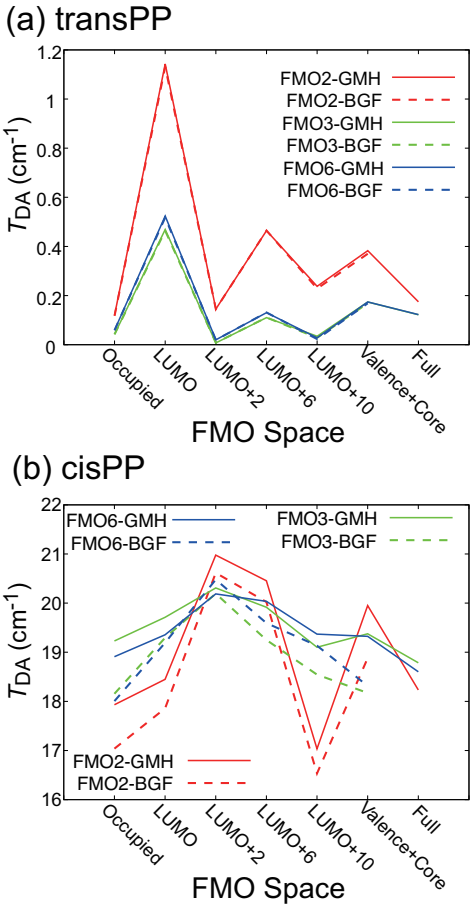

FIG. 3: Transfer matrix element $T_{\rm DA}$ with various rFMO spaces for (a) transPP and (b) cisPP.

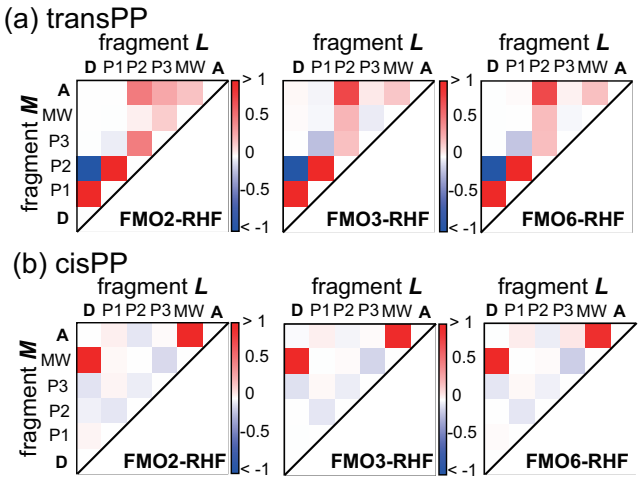

FIG. 4: Normalized inter-fragment tunneling current $\mathcal{K}_{L,M}$ from fragment L to M with FMO2-, FMO3-, and FMO6-LC(VC)MO methods for (a) transPP and (b) cisPP.

Table IV. Transfer matrix element $T_{\rm DA}$ (in cm^{-1}) with various rFMO spaces for transPP complex.

FMO space	FMO2		FMO3		FMO6	
	GMH	BGF	GMH	BGF	GMH	BGF
Full	0.1745	—	0.1219	—	0.1224	—
LC(VC)MO	0.3826	0.3702	0.1738	0.1688	0.1740	0.1687
LUMO+10	0.2375	0.2286	0.03438	0.02850	0.02806	0.02301
LUMO+6	0.4642	0.4646	0.1101	0.1108	0.1303	0.1312
LUMO+2	0.1451	0.1448	0.07364	0.07956	0.0200	0.0195
LUMO	1.143	1.132	0.4641	0.4638	0.5238	0.5176
Occupied	0.1198	0.1173	0.04252	0.04199	0.05932	0.05858

Table V. Same as Table IV but for cisPP complex.

	FMO2		FMO3		FMO6	
	GMH	BGF	GMH	BGF	GMH	BGF
Full	18.23	—	18.79	—	18.60	—
LC(VC)MO	19.95	18.88	19.38	18.17	19.32	18.31
LUMO+10	17.03	16.53	19.10	18.54	19.37	19.13
LUMO+6	22.45	20.02	19.92	19.25	20.04	19.59
LUMO+2	29.98	20.61	20.31	20.19	20.19	20.48
LUMO	18.45	17.86	19.71	19.29	19.36	19.19
Occupied	17.93	17.04	19.23	18.16	18.91	18.01

FMO6.

Interestingly, the results with the occupied space appear closest to those with the full FMO space. We consider this happend as the hole transfer is the principal mechanism for the present system. Thus, the addition of small number of LUMOs could have caused imbalance of description. However, generality of this view should be examined with more cases.

C. ET pathway analysis

Now we examine the ET pathway. Figure 4(a) displays the normalized inter-fragment tunneling currents in transPP, comparing FMO2 and FMO3 with the reference FMO6. In this figure, the LC(VC)MO space was employed. The numerical values are listed in Table S8-S10 of the Supplementary Material. The figure clearly indicates improvement of accuracy with FMO3 over FMO2. The main pathway is the forward ET of D→P1→P2→A, with a bifurcate back-flow of P2→D. The back-flow is due to destructive interference. (See Eq. (13)) The figure indicates that FMO3 and FMO6 exhibit larger back-flow than FMO2, which explains the overestimate of $T_{\rm DA}$ by FMO2 seen in Fig. 3(a).

The corresponding results for cisPP are displayed in Fig. 4(b). The numerical values are listed in Table S11-S13 of the Supplementary Material. The major pathway is the forward flow of D→MW→A. In contrast with transPP, both FMO2 and FMO3 qualitatively reproduce the pathway of reference FMO6 calculation. This implies that, as noted in Sec. IV B, the shorter donor-acceptor distance in cisPP makes the direct pathway dominant, which could have masked the error stemming from the BDAs.

V. CONCLUDING REMARKS

Comparison between cisPP and transPP indicated that the value of $T_{\rm DA}$ is affected notably by the selection of rFMO space. Generally, the three-body correction of FMO3 markedly improved the $T_{\rm DA}$ value. The ET pathway analysis is also made robust by the FMO3 correction, especially when the BDAs are involved in the ET pathway.

We employed the restricted Hartree-Fock (RHF) wave function in this first report. To include electron correlation effects, an efficient way would be with the density functional theory. For instance, we have recently found that the Kohn-Sham orbitals from the long-range corrected functional give accurate electronic coupling energies with non-empirical tuning of the range-separation parameter [18]. The FMO3 correction will also make this scheme versatile. To the correlated wave functions such as the configuration interaction and coupled-cluster, extension of the FMO-LCMO scheme seems less straightforward but deserves further examination.

Acknowledgments

The authors acknowledge support from KAKENHI No. 20108017 ("π-space"). H. K.-N. also acknowledges support from Collaborative Research Program for Young Scientists of ACCMS and IIMC, Kyoto University.

[1] C. C. Moser, J. M. Keske, K. Warncke, R. S. Farid, and P. L. Dutton, Nature **355**, 796 (1992).
[2] P. L. Dutton and C. C. Mosser, Proc. Natl. Acad. Sci. USA **91**, 10247 (1994).
[3] J. R. Winkler, A. J. Di Bilio, N. A. Farrow, J. H. Richards, and H. B. Gray, Pure Appl. Chem. **71**, 1753 (1999).
[4] H. B. Gray and J. R. Winkler, Proc. Natl. Acad. Sci. USA. **102**, 3534 (2005).
[5] O. Farver and I. Pecht, Coord. Chem. Rev. **255**, 757 (2011).
[6] H. M. McConnell, J. Chem. Phys. **35**, 508 (1961).
[7] K. Kitaura, E. Ikeo, T. Asada, T. Nakano, and M. Uebayasi, Chem. Phys. Lett. **313**, 701 (1999).
[8] D. G. Fedorov and K. Kitaura, J. Phys. Chem. A **111**, 6904 (2007).
[9] S. Tanaka, Y. Mochizuki, Y. Komeiji, Y. Okiyama, and K. Fukuzawa, Phys. Chem. Chem. Phys. **16**, 10310 (2014).
[10] W. Yang and T. S. Lee, J. Chem. Phys. **103**, 5674 (1995).
[11] T. Akama, M. Kobayashi, and H. Nakai, Int. J. Quant. Chem. **109**, 2706 (2009).
[12] W. Li and P. Piecuch, J. Phys. Chem. A **114**, 6721 (2010).
[13] Y. Aoki and F. L. Gu, Phys. Chem. Chem. Phys. **14**, 7640 (2012).

[14] M. S. Gordon, D. G. Fedorov, S. R. Pruitt, and L. V. Slipchenko, Chem. Rev. **112**, 632 (2012).

[15] K. Raghavachari and A. Saha, Chem. Rev. **115**, 5643 (2015).

[16] H. Nishioka and K. Ando, J. Chem. Phys. **134**, 204109 (2011).

[17] H. Kitoh-Nishioka and K. Ando, J. Phys. Chem. B **116**, 12933 (2012).

[18] H. Kitoh-Nishioka and K. Ando, Chem. Phys. Lett. **621**, 96 (2015).

[19] S. Tsuneyuki, T. Kobori, K. Akagi, K. Sodeyama, K. Terakura, and H. Fukuyama, Chem. Phys. Lett. **476**, 104 (2009).

[20] T. Kobori, K. Sodeyama, T. Otsuka, Y. Tateyama, and S. Tsuneyuki, J. Chem. Phys. **139**, 094113 (2013).

[21] A. Szabo and N. S. Ostlund, *Modern Quantum Chemistry* (Dover, New York, 1996).

[22] S. S. Isied, M. Y. Ogawa, and J. F. Wishart, Chem. Rev. **92**, 381 (1992).

[23] M. Y. Ogawa, J. F. Wishart, Z. Young, J. R. Miller, and S. S. Isied, J. Phys. Chem. **97**, 11456 (1993).

[24] M. Y. Ogawa, I. Moreira, J. F. Wishart, and S. S. Isied, Chem. Phys. **176**, 589 (1993).

[25] F. Wallrapp, A. A. Voityuk, and V. Guallar, J. Chem. Theory Comput. **5**, 3312 (2009).

[26] F. Wallrapp, A. A. Voityuk, and V. Guallar, J. Chem. Theory Comput. **6**, 3241 (2010).

[27] R. J. Cave and M. D. Newton, Chem. Phys. Lett. **249**, 15 (1996).

[28] S. S. Skourtis and D. N. Beratan, Adv. Chem. Phys. **106**, 377 (1999).

[29] J. J. Regan and J. N. Onuchic, Adv. Chem. Phys. **107**, 497 (1999).

[30] A. A. Stuchebrukhov, Theor. Chem. Acc. **110**, 291 (2003).

[31] A. A. Stuchebrukhov, J. Chem. Phys. **105**, 10819 (1996).

[32] S. Grimme, J. Antony, S. Ehrlich, and H. Krieg, J. Chem. Phys. **132**, 154104 (2010).

[33] M. J. Frisch, G. W. Trucks, H. B. Schlegel, G. E. Scuseria, M. A. Robb, J. R. Cheeseman, G. Scalmani, V. Barone, B. Mennucci, G. A. Petersson, et al., *Gaussian 09 Revision D.01*, Gaussian Inc. Wallingford CT 2013.

[34] M. W. Schmidt, K. K. Baldridge, J. A. Boatz, S. T. Elbert, M. S. Gordon, J. H. Jensen, S. Koseki, N. Matsunaga, K. A. Nguyen, S. Su, et al., J. Comput. Chem. **14**, 1347 (1993).

[35] D. G. Fedorov and K. Kitaura, J. Chem. Phys. **120**, 6832 (2004).

[36] T. Nakano, T. Kaminuma, T. Sato, K. Fukuzawa, Y. Akiyama, M. Uebayasi, and K. Kitaura, Chem. Phys. Lett. **351**, 475 (2002).

Supplementary Material

Optimized Structures

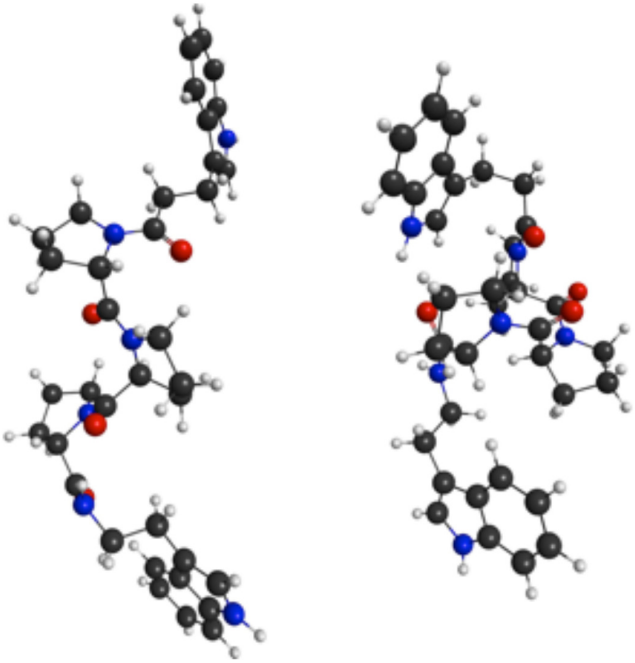

Fig.S1 Optimized structures of transPP (left) and cisPP (right) at the B3LYP/6-31G(d)-D3 level. Cartesian coordinates are tabulated in Table S1 next page.

Table S1. Cartesian coordinates (in Å) of the structures in Fig.S1.

	transPP			cisPP		
C	-5.372434	-0.248416	0.062586	-4.971844	1.699604	0.475856
H	-5.223344	-0.044113	1.132175	-5.246735	1.306885	1.457460
C	-5.735621	-1.728813	-0.135761	-5.603116	0.816940	-0.639827
H	-5.854165	-1.918929	-1.209884	-6.666165	0.676488	-0.407233
H	-4.890183	-2.346251	0.183729	-5.569017	1.352615	-1.594752
C	-6.981602	-2.109259	0.607296	-4.909142	-0.504208	-0.784947
C	-7.071459	-2.893518	1.729218	-3.824857	-0.753603	-1.587351
C	-8.326197	-1.681855	0.304662	-5.123114	-1.702775	-0.013530
H	-6.288511	-3.406216	2.271782	-3.309798	-0.095425	-2.272372
N	-8.389735	-2.978996	2.146910	-3.373190	-2.045405	-1.405494
C	-9.184333	-2.246872	1.289035	-4.130589	-2.642560	-0.416482
C	-8.887866	-0.883154	-0.706502	-6.043564	-2.069266	0.981646
H	-8.719400	-3.517801	2.931645	-2.435580	-2.309688	-1.675676
C	-10.566610	-2.032309	1.287072	-4.041872	-3.917355	0.152543
C	-10.260725	-0.666079	-0.713117	-5.953903	-3.333529	1.553712
H	-8.256084	-0.447998	-1.476867	-6.809389	-1.368331	1.305246
H	-11.207086	-2.472724	2.046967	-3.281526	-4.624352	-0.168891
C	-11.091445	-1.234430	0.275610	-4.960624	-4.247624	1.144668
H	-10.705317	-0.051496	-1.491208	-6.656798	-3.624582	2.329844
H	-12.161447	-1.047689	0.245609	-4.913849	-5.228879	1.609710
H	-6.206356	0.395328	-0.245078	-5.349846	2.726995	0.398016
C	5.537765	-0.621081	-0.911341	3.744816	-1.563074	-2.100025
H	4.971085	-0.715441	0.024180	3.283052	-2.318982	-1.451355
H	4.835236	-0.809198	-1.733596	3.749375	-1.983068	-3.112937
C	6.657992	-1.613750	-0.915526	5.134565	-1.259284	-1.628448
C	7.020002	-2.495988	-1.901059	6.241302	-0.985179	-2.393681
C	7.604525	-1.790364	0.159501	5.535237	-1.082933	-0.253496
H	6.565291	-2.676172	-2.866018	6.356238	-1.003598	-3.469127
N	8.136541	-3.215375	-1.503844	7.305888	-0.646955	-1.578659
C	8.515820	-2.804473	-0.240758	6.903724	-0.697270	-0.258887
C	7.753870	-1.183072	1.419283	4.875484	-1.224726	0.980385
H	8.586623	-3.937864	-2.042346	8.237522	-0.431243	-1.896542
C	9.565340	-3.227275	0.582218	7.611976	-0.439028	0.919660
C	8.796993	-1.601414	2.237659	5.572622	-0.966457	2.154456
H	7.068708	-0.399383	1.735028	3.839319	-1.549788	1.018992
H	10.255656	-4.004976	0.265163	8.657608	-0.143881	0.896502
C	9.691445	-2.611843	1.823798	6.927450	-0.573215	2.122706
H	8.929918	-1.143033	3.213926	5.071528	-1.072891	3.112393
H	10.496578	-2.915789	2.487619	7.447318	-0.377366	3.056129
C	-4.107769	0.141384	-0.692792	-3.449532	1.661316	0.436860
O	-3.389861	-0.693300	-1.249382	-2.802119	1.024540	1.265214
N	-3.801938	1.468648	-0.723001	-2.822496	2.292208	-0.603441
C	-4.519514	2.557257	-0.047672	-3.397580	3.231957	-1.573137
H	-4.764988	2.287502	0.984086	-3.932046	4.043672	-1.069119
H	-5.460105	2.778722	-0.572427	-4.102053	2.716797	-2.237671
C	-3.538067	3.737284	-0.122149	-2.174605	3.756137	-2.354794
H	-4.052467	4.702717	-0.143263	-1.834151	4.693190	-1.908457
H	-2.865474	3.705951	0.737251	-2.402315	3.931080	-3.410844
C	-2.732507	3.454760	-1.402036	-1.104717	2.669638	-2.140698
H	-1.764747	3.963334	-1.416004	-0.083775	3.037010	-2.287694
H	-3.293969	3.765528	-2.291050	-1.262660	1.817426	-2.813270
C	-2.585924	1.918316	-1.410697	-1.370078	2.210431	-0.693736
H	-2.575908	1.509928	-2.421824	-1.071216	1.177799	-0.518523
C	-1.347668	1.475309	-0.612773	-0.719984	3.190884	0.306623
O	-1.211397	1.849419	0.559113	-1.248364	4.274252	0.548583
N	-0.425028	0.704236	-1.232154	0.495515	2.857868	0.824329
C	-0.518913	0.088221	-2.570280	1.140211	3.740198	1.810419
H	-0.646138	0.853719	-3.341947	0.401122	4.081791	2.539089
H	-1.380965	-0.585728	-2.588841	1.540597	4.625377	1.300008
C	0.818137	-0.652447	-2.724359	2.244349	2.866828	2.426730
H	1.566848	0.017207	-3.152519	1.859688	2.365842	3.317980
H	0.721278	-1.536875	-3.361159	3.132182	3.444693	2.700144
C	1.212747	-0.997368	-1.279471	2.534078	1.818781	1.337580
H	2.284841	-1.177909	-1.158622	3.019520	0.915849	1.719994
H	0.674035	-1.886868	-0.934171	3.180702	2.238175	0.556884
C	0.728401	0.219704	-0.462839	1.137358	1.545298	0.740190
H	0.397879	-0.071293	0.533795	1.200129	1.236721	-0.305125
C	1.814560	1.304093	-0.407202	0.350024	0.519602	1.585136
O	2.311270	1.711646	-1.469698	-0.063050	0.816286	2.696782
N	2.245189	1.734611	0.801642	0.109003	-0.701920	1.012846
C	1.581920	1.574677	2.109101	-0.750283	-1.664897	1.725561
H	2.073360	0.778692	2.683633	-1.771668	-1.277435	1.751920
H	0.525249	1.351333	1.973216	-0.396251	-1.773778	2.757907
C	1.805101	2.945368	2.756388	-0.590345	-2.955249	0.916101
H	1.703337	2.913972	3.845414	-1.327142	-2.982617	0.113673
H	1.060574	3.646428	2.361153	-0.721310	-3.850699	1.529849
C	3.221796	3.325949	2.296659	0.825265	-2.842544	0.326309
H	3.975112	2.859595	2.938198	0.983704	-3.473377	-0.553830
H	3.396902	4.405422	2.291320	1.578495	-3.112561	1.076192
C	3.348782	2.725557	0.885964	0.969153	-1.333235	0.007007
H	3.202190	3.464481	0.091699	2.000997	-1.012468	0.151305
C	4.686718	1.977699	0.671114	0.520111	-1.046805	-1.437526
O	5.354509	1.553037	1.612600	-0.626555	-1.281195	-1.817467
N	5.017290	1.802128	-0.636757	1.444859	-0.531755	-2.301209
H	4.254915	1.953291	-1.295434	1.091646	-0.444695	-3.247304
C	6.048153	0.837217	-0.993796	2.868322	-0.289928	-2.077600
H	6.883713	0.972767	-0.304518	3.009560	0.233150	-1.127806
H	6.406451	1.060567	-2.003641	3.208838	0.401611	-2.854122

Electron transfer energy

transPP complex

Table S2. MO energy gap, maximum absolute error (MAE), root-mean-squares (RMS) error, and transfer matrix element T_{DA} with FMO2-LCMO method for transPP complex.

	Gap (eV)	MAE (eV)		RMS (eV)		T_{DA} (cm^{-1})	
		Occ	Uoc	Occ	Uoc	GMH	BGF
Full	10.66	0.195	0.218	0.0399	0.0508	0.1745	—
LC(VC)MO	10.66	0.107	22.4	0.0345	3.92	0.3826	0.3702
LUMO+10	10.66	0.218	20.6	0.0479	4.53	0.2375	0.2286
LUMO+6	10.66	0.231	12.9	0.0521	3.52	0.4642	0.4646
LUMO+2	10.65	0.243	6.20	0.0563	2.01	0.1451	0.1448
LUMO	10.65	0.256	2.97	0.0600	1.22	1.143	1.132
Occupied	—	0.257	—	0.0620	—	0.1198	0.1173

Table S3. Same as Table S2 but with FMO3-LCMO.

	Gap (eV)	MAE (eV)		RMS (eV)		T_{DA} (cm^{-1})	
		Occ	Uoc	Occ	Uoc	GMH	BGF
Full	10.67	0.0400	0.0293	0.0119	0.0080	0.1219	—
LC(VC)MO	10.67	0.102	14.6	0.0266	3.12	0.1738	0.1688
LUMO+10	10.67	0.167	18.6	0.0383	4.27	0.03438	0.02850
LUMO+6	10.67	0.179	13.2	0.0432	3.32	0.1101	0.1108
LUMO+2	10.66	0.191	5.69	0.0479	1.87	0.07364	0.07956
LUMO	10.66	0.216	2.39	0.0515	1.10	0.4641	0.4638
Occupied	—	0.232	—	0.0534	—	0.04252	0.04199

Table S4. Same as Table S2 but with FMO6-LCMO, i.e., for the entire Trp-$(\mathrm{Pro})_3$-Trp system.

	Gap (eV)	MAE (eV)		RMS (eV)		T_{DA} (cm^{-1})	
		Occ	Uoc	Occ	Uoc	GMH	BGF
Full	10.63	—	—	—	—	0.1224	—
LC(VC)MO	10.63	0.0934	14.6	0.0223	3.13	0.1740	0.1687
LUMO+10	10.63	0.179	18.6	0.0352	4.27	0.02806	0.02301
LUMO+6	10.63	0.192	13.2	0.0400	3.32	0.1303	0.1312
LUMO+2	10.62	0.203	5.71	0.0451	1.87	0.0200	0.0195
LUMO	10.62	0.220	2.39	0.0489	1.09	0.5238	0.5176
Occupied	—	0.235	—	0.0508	—	0.05932	0.05858

cisPP complex

Table S5. Same as Table S2 but for cisPP complex.

	Gap (eV)	MAE (eV)		RMS (eV)		T_{DA} (cm^{-1})	
		Occ	Uoc	Occ	Uoc	GMH	BGF
Full	9.880	0.215	0.356	0.0571	0.0724	18.23	—
LC(VC)MO	9.885	0.271	22.2	0.0504	3.74	19.95	18.88
LUMO+10	9.890	0.370	26.1	0.0610	4.93	17.03	16.53
LUMO+6	9.894	0.405	15.0	0.0683	3.56	22.45	20.02
LUMO+2	9.912	0.416	9.34	0.0712	2.86	20.98	20.61
LUMO	9.924	0.426	5.42	0.0752	2.01	18.45	17.86
Occupied	—	0.443	—	0.0782	—	17.93	17.04

Table S6. Same as Table S5 but with FMO3-LCMO.

	Gap (eV)	MAE (eV)		RMS (eV)		T_{DA} (cm^{-1})	
		Occ	Uoc	Occ	Uoc	GMH	BGF
Full	9.886	0.0405	0.124	0.0096	0.0156	18.79	—
LC(VC)MO	9.890	0.0988	14.9	0.0227	3.12	19.38	18.17
LUMO+10	9.900	0.172	21.3	0.0361	4.58	19.10	18.54
LUMO+6	9.905	0.199	14.1	0.0449	3.30	19.92	19.25
LUMO+2	9.926	0.224	7.92	0.0485	2.35	20.31	20.19
LUMO	9.935	0.278	4.38	0.0532	1.64	19.71	19.29
Occupied	—	0.294	—	0.0558	—	19.23	18.16

Table S7. Same as Table S5 but with FMO6-LCMO.

	Gap (eV)	MAE (eV)		RMS (eV)		T_{DA} (cm^{-1})	
		Occ	Uoc	Occ	Uoc	GMH	BGF
Full	9.909	—	—	—	—	18.60	—
LC(VC)MO	9.909	0.0863	14.9	0.0213	3.14	19.32	18.31
LUMO+10	9.919	0.170	21.2	0.0361	4.58	19.37	19.13
LUMO+6	9.924	0.208	14.0	0.0455	3.31	20.04	19.59
LUMO+2	9.946	0.235	8.26	0.0493	2.41	20.19	20.48
LUMO	9.955	0.284	4.41	0.0541	1.66	19.36	19.19
Occupied	—	0.307	—	0.0567	—	18.91	18.01

Normalized tunneling current

transPP helix

Table S8. Normalized tunneling current in transPP with FMO2-LC(VC)MO.

	D	P1	P2	P3	MW
P1	2.012				
P2	-1.011	2.054			
P3	-0.002	-0.042	0.492		
MW	0.000	0.000	0.046	0.149	
A	0.000	0.000	0.506	0.300	0.194

Table S9. Same as Table S8 but with FMO3-LC(VC)MO.

	D	P1	P2	P3	MW
P1	3.496				
P2	-2.534	3.738			
P3	0.006	-0.197	0.201		
MW	0.014	-0.020	0.237	-0.053	
A	0.018	-0.024	0.766	0.062	0.178

Table S10. Same as Table S8 but with FMO6-LC(VC)MO.

	D	P1	P2	P3	MW
P1	3.531				
P2	-2.521	3.694			
P3	-0.007	-0.179	0.204		
MW	-0.002	0.006	0.213	-0.018	
A	-0.001	0.010	0.755	0.037	0.198

cisPP helix

Table S11. Same as Table S8 but for cisPP complex.

	D	P1	P2	P3	MW
P1	0.025				
P2	-0.035	-0.067			
P3	-0.073	0.029	-0.043		
MW	1.082	0.021	0.007	-0.104	
A	0.002	0.043	-0.066	0.015	1.006

Table S12. Same as Table S11 but with FMO3-LC(VC)MO.

	D	P1	P2	P3	MW
P1	-0.003				
P2	0.003	-0.064			
P3	-0.084	0.019	-0.045		
MW	1.091	-0.004	0.009	-0.123	
A	-0.008	0.046	-0.025	0.013	0.973

Table S13. Same as Table S11 but with FMO6-LC(VC)MO.

	D	P1	P2	P3	MW
P1	0.009				
P2	0.001	-0.067			
P3	-0.067	0.023	-0.035		
MW	1.060	0.001	0.010	-0.142	
A	-0.003	0.052	-0.040	0.063	0.928